K-shell double photoionization of Be, Mg, and Ca

A. S. Kheifets[*]

Research School of Physical Sciences, The Australian National University, Canberra ACT 0200, Australia

Igor Bray

ARC Centre for Matter-Antimatter Studies, Curtin University, WA 6845 Perth, Australia

J. Hoszowska

Department of Physics, University of Fribourg, CH-1700 Fribourg, Switzerland

We perform convergent close-coupling calculations of double photoionization (DPI) of the *K*-shell of alkaline-earth metal atoms (Be, Mg, and Ca) from the threshold to the nonrelativistic limit of infinite photon energy. Theoretical double-to-single photoionization cross-section ratios for Mg and Ca are compared with experimental values derived from high-resolution x-ray spectra following the radiative decay of the *K*-shell double vacancy. We investigate the role of many-electron correlations in the ground and doubly-ionized final states played in the DPI process. Universal scaling of DPI cross section with an effective nuclear charge is examined in neutral atoms in comparison with corresponding heliumlike ions.

I. INTRODUCTION

Direct double photoionization (DPI) of atoms initiated by absorption of a single photon is a fundamental process driven entirely by many-electron correlation. Due to its fundamental importance, it has attracted considerable interest from theory and experiment alike [1,2]. Most of these studies focused on the valence shell DPI. In comparison, less attention was given to DPI of the innermost *K* shell. With the advent of intense and energy tunable x-ray synchrotron sources, the investigation of the photon energy dependence of the double $1s$ vacancy production became accessible. Experimentally, one measures the intensity ratio of the hypersatellite $K\alpha_2^h$ ($1s^{-2} \rightarrow 1s^{-1}2p^{-1}$) and the diagram $K\alpha$ ($1s^{-1} \rightarrow 2p^{-1}$) x-ray emission lines. When this ratio is corrected for the fluorescence yields of the single-hole state ω_K and the double-hole state ω_{KK}, it can be converted into the double-to-single *K*-shell photoionization cross-section ratio

$$P_{KK} = \frac{I_{K\alpha_2^h}}{I_{K\alpha}} \frac{\omega_K}{\omega_{KK}}. \tag{1}$$

Due to a rather soft, in the perturbation sense, nature of electron-photon interaction, the probability for creating *K*-shell double vacancy by photon impact is quite low ($10^{-2} - 10^{-6}$). As a consequence, experimental data are scarce with most of the experimental results available for the $3d$ transition elements [3,4]. The double *K*-shell vacancy production at several photon energies from threshold to the expected maximum was also investigated for Ag [5]. For light elements beyond helium $2 < Z \leq 20$, the only measurement performed by means of high-resolution Auger-electron spectroscopy was reported for Ne at a fixed photon energy of 5 keV [6]. Oura *et al.* [3] measured the P_{KK} ratio in Ca in the

photon energy range of 8–20 keV. This ratio was compared with the theoretical double-to-single photoionization cross-section ratio from a perturbation-theory calculation [7].

Very recently, Hoszowska *et al.* [8] investigated the evolution of P_{KK} over a wide range of photon energies from the threshold up and beyond the P_{KK} maximum in Mg, Al, and Si. The P_{KK} ratio was converted into the DPI cross-section $\sigma^{2+} = P_{KK}\sigma^+$ by using the single *K*-shell photoionization cross-section values σ^+ from the XCOM database [9]. Hoszowska *et al.* [8] analyzed the DPI cross section as a function of the excess energy above the threshold in the reduced coordinates $\sigma^{2+} Z^{*4}$ vs $\Delta E/Z^{*2}$ and established a universal scaling law similar to the one suggested by Kornberg and Miraglia [10] for the helium isoelectronic sequence of ions. The effective nucleus charge Z^* was derived from the binding energy of the remaining *K*-shell electron using the hydrogenic formula $\epsilon_{1s^+} = Z^{*2}$ Ry, where Ry = 13.6 eV. For the heliumlike targets $Z^* = Z$. The scaled $\sigma^{2+} Z^{*4}$ curve for neutral atoms was markedly below the $\sigma^{2+} Z^4$ curve for the corresponding heliumlike ions [11]. However, the scaling with a slightly different exponent $\sigma^{2+} Z^{*3.68}$ for neutral atoms allowed to match the corresponding DPI cross sections of the He-like ions scaled with the bare charges.

Huotari *et al.* [4] performed a similar scaling of their experimental P_{KK} ratios in the $3d$ transition-metal atoms $23 \leq Z \leq 30$. The common energy scale was expressed in units of $\Delta E/\epsilon_{1s^+}$ with $\epsilon_{1s^+} = E_{th} - E_K$ being determined by the difference between the DPI threshold E_{th} and the *K*-edge energy E_K. The P_{KK} ratios were normalized to unity near the saturation. Thus produced a universal curve was found to be very close to the theoretical predictions based on the knock-out (KO) mechanism of the DPI in He [12].

Apart from this semiempirical analysis of experimental data, theoretical studies of the *K*-shell DPI were limited, for the most part, to the asymptotic regime of very large photon energies. In this regime, for the helium isoelectronic sequence of ions, the double-to-single photoionization cross-

*Corresponding author; a.kheifets@.anu.edu.au

section ratio can be calculated quite accurately provided that electron correlation is accounted for in the initial-state wave function [13]. Mikhailov *et al.* [7] investigated the double K-shell ionization of heliumlike ions within the lowest-order perturbation theory (LOPT). They compared the ratio of double-to-single photoionization cross sections with available experimental data for a number of neutral atoms at a single fixed photon energy point. Generally, a good agreement was reported between theory and experiment. In the case of Ca, a comparison was made over a wide photon energy range from the threshold to the broad cross-section ratio maximum where the theory was noticeably below the experimental P_{KK} values of Oura *et al.* [3]. Few lowest members of the helium isoelectronic sequence $1 \leq Z \leq 6$ were investigated in a wide photon energy range, from the threshold to the nonrelativistic limit of infinite photon energy, within a nonperturbative convergent close-coupling (CCC) approach [11]. The universal Z-scaling suggested by Kornberg and Miraglia [10] was supported by this calculation.

Experimental results and semiempirical analysis by Hoszowska *et al.* [8] suggested that the effect of electron correlations on the K-shell DPI of low-Z atoms is quite different in comparison with corresponding heliumlike ions. In the meantime, to the best knowledge of the authors, there have been no reports on *ab initio* nonperturbative calculations of the K-shell DPI of neutral atomic targets. Such a calculation is attempted in the present work. We focus our attention on the alkaline-earth metal atoms (Be, Mg, and Ca) for which the CCC formalism, developed originally for heliumlike two-electron targets, can be readily generalized. We demonstrated this in a recent calculation of the valence shell DPI [14]. Our theoretical results for Be and Mg were found to be in a good agreement with experimental data over a wide range of photon energies [15,16].

In the K-shell DPI study, we employ the same frozen-core model with two active ns^2 electrons which we used previously for the valence shell DPI calculation. This is justified since the innermost K-shell is well separated, both in the coordinate space and energy, from the rest of the atom. As to the subsequent radiative transitions giving rise to x-ray fluorescence, they are believed to be delayed with respect to the DPI process, and their effect thus can be neglected.

II. THEORETICAL MODEL

A. Atomic ground state

Adequate account for the ground-state correlation is important for accurate theoretical description of the DPI process [17]. In the present work, we employed a multiconfiguration Hartree-Fock (MCHF) expansion of the ground-state wave function generated with a computer code by Dyall *et al.* [18]. In the MCHF expansion, the dominant $1s^2$ configuration is supplemented by a number of nl^2 terms representing unoccupied orbitals above the Fermi level,

$$\Psi_0(\boldsymbol{r}_1, \boldsymbol{r}_2) = C_{1s} \langle \boldsymbol{r}_1 \boldsymbol{r}_2 | 1s^2 \rangle + \sum_{\epsilon_{nl} > E_F} C_{nl} \langle \boldsymbol{r}_1 \boldsymbol{r}_2 | nl^2 \rangle. \quad (2)$$

These added terms are optimized to give the lowest ground-state energy. The occupied atomic orbitals above the K shell

TABLE I. The first, second, and double-ionization potentials (in keV) of the K shells of Be, Mg, and Ca calculated with various ground-state wave functions and compared with experimental values. The effective charge Z^* is derived from the second ionization potential using the hydrogenic formula.

Ground state	K-shell ionization potentials (keV)			Z^*
	First	Second	Double	
Beryllium				
MCHF-13	0.124	0.180	0.305	3.64
Jastrow [20]			0.303	
LeSech [19]			0.319	
Magnesium				
MCHF-11	1.310	1.462	2.772	10.37
MCDF [8]	1.312	1.465	2.777	
LeSech [19]			2.848	
Experiment [8]			2.741	
Calcium				
MCHF7	4.032	4.302	8.334	17.78
MCDF [3]			8.357	
Experiment [8]			8.039	
Experiment [3]			8.11	

are treated as a frozen core and are not included into the MCHF expansion. We kept only those terms in Eq. (2) for which $C_{nl} \geq 10^{-4}$, thus generating MCHF expansions with 13, 11, and 7 terms for Be, Mg, and Ca. Decreasing number of terms indicates weakening of correlation in the K shell with the increase in the nucleus charge Z. To study the role of the ground-state correlation in the DPI process, we performed some of our calculations with a single-configuration Hartree-Fock (HF) wave function by setting $C_{1s} = 1$ in Eq. (2) and discarding all other terms.

As an alternative method, we tried a correlated wave function of the LeSech (LeS)-type suggested by Mitnik and Miraglia [19],

$$\Psi_0(\boldsymbol{r}_1, \boldsymbol{r}_2) = N \frac{Z^3}{\pi} e^{-Zr_1} e^{-Zr_2} \cosh(\alpha r_1)$$
$$\times \cosh(\alpha r_2) \left[1 + \frac{1}{2} r_{12} e^{-\lambda r_{12}} \right]. \quad (3)$$

Even though these authors did not specify explicit values of the LeS parameters for Mg or Ca, we were able to find these parameters by the fourth power polynomial interpolation from available data for neighboring Z atoms.

The total energies of neutral atomic species and the corresponding singly- and doubly-charge ions with one and two K-shell vacancies were used to calculate the first, second, and double-ionization potentials which are presented in Table I. For comparison, in the same table, we display analogous

TABLE II. Double-to-single photoionization cross-section ratio $R = \sigma^{2+}/\sigma^+|_{\omega \to \infty}$ of the neutral atoms Be, Mg, Ca and heliumlike ions Be^{2+} and Mg^{10+} calculated with various ground states.

GS	Neutral atoms			He-like ions	
	Be	Mg	Ca	Be^{2+}	Mg^{10+}
HF	0.687	0.068	0.025		
MCHF	1.289	0.123	0.043	0.533	
LeS	1.199	0.085	0.031		
Hyl				0.564	0.062

data obtained with other types of the ground-state wave function as well as experimental K-shell double-ionization potentials.

Another useful characteristic of the ground state is an asymptotic double-to-single photoionization cross-section ratio $R = \sigma^{2+}/\sigma^+|_{\omega \to \infty}$ calculated in the limit of the infinite photon energy. It can be evaluated according to the nonrelativistic expressions of Dalgarno and Stewart [21],

$$\sigma_n \propto \langle \phi_n | \psi \rangle, \quad \sigma_t \propto \langle \psi | \psi \rangle, \quad \sigma^+ = \sum_{\epsilon_n > E_F}^{\infty} \sigma_n, \quad \sigma^{2+} = \sigma_t - \sigma^+.$$
(4)

Here $\psi(\mathbf{r}_1) = \Psi_0(\mathbf{r}_1, \mathbf{r}_2 = 0, \mathbf{r}_{12} = \mathbf{r}_1)$ and $\phi_n(\mathbf{r}_1)$ is the $l = 0$ eigenstate with the principal quantum number n. Thus defined R ratios for the K shells of neutral Be, Mg, and Ca calculated with various ground-state wave functions are presented in Table II. For comparison, we show the analogous ratios for the corresponding heliumlike ions Be^{2+} and Mg^{10+} calculated with a 20 parameter Hylleraas (Hyl) ground states due to Hart and Herzberg [22].

Mitnik and Miraglia [19] suggested that the influence of passive outer-shell electrons on electron-electron correlation should be very small. The outer-shell electrons affect the electron-nucleus interaction but not the electron-electron interaction. According to this scenario, the photoabsorption asymptotic ratios for the neutral atoms and the corresponding heliumlike ions should be very similar. In Table II we see that the ion ratios are indeed close to those of the least correlated HF ground state of the corresponding neutral atomic species. This similarity largely disappears when the comparison is made with more correlated MCHF or LeS ground state.

B. Two-electron continuum

We use the multichannel expansion for the final-state wave function of the two-electron system,

$$\langle \Psi_j^{(-)}(\mathbf{k}_b)| = \langle \mathbf{k}_b^{(-)} j| + \sum_i \oint d^3k \frac{\langle \mathbf{k}_b^{(-)} j|T|i\mathbf{k}^{(+)}\rangle \langle \mathbf{k}^{(+)} i|}{E - \varepsilon_k - \epsilon_i + i0}, \quad (5)$$

with boundary conditions corresponding to an outgoing wave in a given channel $\langle \mathbf{k}_b^{(-)} j|$ and incoming waves in all other channels $|i\mathbf{k}^{(+)}\rangle$. Here $E = k_b^2/2 + \epsilon_j$ is the final-state energy. The channel wave function $\langle \mathbf{k}_b^{(-)} j|$ is the product of a one-

electron orbital $\bar{\phi}_j$ with energy ϵ_j, obtained by diagonalizing the target Hamiltonian in a Laguerre basis, and a (distorted) Coulomb outgoing wave $\chi^{(-)}(\mathbf{k}_b)$ with energy ε_k. The asymptotic charge seen by the Coulomb wave is unity which results from the screening of the nucleus charge Z by the $Z - 1$ electrons. The half off-shell T-matrix in Eq. (5) is the solution of the corresponding Lippmann-Schwinger integral equation [23]

$$\langle \mathbf{k}^{(+)} i|T|j\mathbf{k}_b^{(-)}\rangle = \langle \mathbf{k}^{(+)} i|V|j\mathbf{k}_b^{(-)}\rangle$$
$$+ \sum_{i'} \oint d^3k' \frac{\langle \mathbf{k}^{(+)} i|V|i'\mathbf{k}'^{(-)}\rangle \langle \mathbf{k}'^{(-)} i'|T|j\mathbf{k}_b^{(-)}\rangle}{E - \varepsilon_{k'} - \epsilon_{i'} + i0}.$$
(6)

The photoionization cross section, as a function of the photon energy ω, corresponding to a particular bound-electron state j is given by [24]

$$\sigma_j(\omega) = \frac{4\pi^2}{\omega c} \sum_{m_j} \int d^3k_b |\langle \Psi_j^{(-)}(\mathbf{k}_b)|\mathcal{D}|\Psi_0\rangle|^2 \delta(\omega - E + E_0),$$
(7)

where $c \simeq 137$ is the speed of light in atomic units. The negative- and positive-energy pseudostates contribute to single and double photoionization cross sections, respectively,

$$\sigma^+ = \sum_{\epsilon_j < 0} \sigma_j, \quad \sigma^{2+} = \sum_{\epsilon_j > 0} \sigma_j. \quad (8)$$

The dipole electromagnetic operator $\mathcal{D}$ can be written in one of the following forms commonly known as length, velocity, and acceleration [24]:

$$\mathcal{D}^r = \omega(z_1 + z_2), \quad \mathcal{D}^\nabla = \nabla_{z_1} + \nabla_{z_2}, \quad \mathcal{D}^{\dot{\nabla}} = Z\omega^{-1}(z_1/r_1^3 + z_2/r_2^3),$$
(9)

with the z axis chosen along the polarization vector of the photon. Convergence, or lack of thereof, between calculations in different gauges serves as a useful test on the accuracy of the initial- and final-state wave functions. By combining the same set of CCC final-state wave functions with various descriptions of the ground state, we can compare the relative accuracy of various ground-state wave functions.

III. EXPERIMENT

High-resolution x-ray emission spectroscopy and x-ray synchrotron radiation were used to investigate the photon energy evolution of the K-shell double vacancy production in Mg and Ca. Experiments have been carried out at two undulator beam lines, ID21 and ID26, at the European Synchrotron Radiation Facility (ESRF), Grenoble, France, employing the Fribourg von Hamos Bragg-type curved crystal spectrometer [25]. The double-to-single photoionization cross-section ratios P_{KK} were deduced from the relative intensities of the resolved hypersatellite $K\alpha^h$ to the diagram $K\alpha$ x-ray transitions. The x-ray emission spectra of Mg were measured using a TlAP(001) crystal in second order and those of Ca
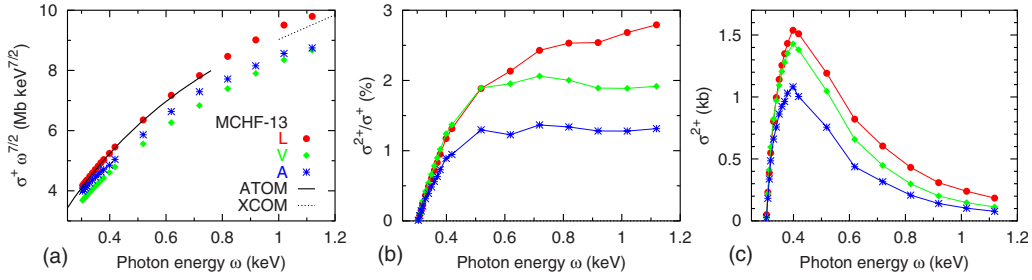
FIG. 1. (Color online) Photoionization cross sections of the K shell of beryllium calculated with the MCHF-13 ground state. Calculations in three gauges of the electromagnetic operator are displayed with red circles (length), green diamonds (velocity), and blue asterisks (acceleration). Single photoionization cross section calculated with the ATOM program suite [26] is shown by the black solid line. The data from XCOM database [9] are shown by the dotted line

with a Ge(220) crystal. The diffracted x-rays were recorded with a position-sensitive back-illuminated charged coupled device (CCD) camera. Intensities of the hypersatellite and diagram x-ray emission lines were corrected for the sample self-absorption and absorption of the incident x-rays, the photon flux, the spectrometer solid angle, as well as for the CCD detector quantum efficiency. The incident photon flux was $\sim 1-3 \times 10^{12}$ photon/s. The Mg data were reported partially in our preceding publication [8] whereas the Ca data are new.

IV. CALCULATION RESULTS

A. Beryllium

Photoionization cross sections of the K shell of beryllium calculated with a MCHF-13 ground state are presented in Fig. 1. Three panels, from left to right, display the single photoionization cross-section $\omega^{7/2}\sigma^+$, compensated by an extra power factor for the fast drop with the photon energy, the double-to-single photoionization cross-section ratio σ^{2+}/σ^+, and the DPI cross-section σ^{2+}. Single photoionization cross section on the left panel is compared with the Hartree-Fock calculation performed with the ATOM program suite [26] and the XCOM data [9] available for photon energies above 1 keV.

We note that the XCOM data refer to the total photoionization cross section summed over all atomic shells. For atoms with the K-shell DPI threshold above 1 keV, the contributions of other shells can be subtracted by an extrapolation procedure. Unfortunately, this was not possible for Be with the DPI threshold of only 0.3 keV. Thus, the true K-shell photoionization cross section is somewhat below the XCOM data drawn in Fig. 1.

Calculations in three gauges of the electromagnetic operator are displayed in the figure: the length, velocity, and acceleration. We learned from our past experience that the length gauge is the most demanding to the quality of the ground state. As seen from Eq. (9), it enhances the contribution of the large distances to the radial integrals where the variational ground-state wave function is inherently inaccurate. On the other hand, the radial integrals in the acceleration gauge are strongly skewed toward the small distances near the nucleus where the ground-state wave function is formed largely by a strong Coulomb force. In comparison

with the two other gauges, the velocity gauge is the best overall performer in DPI calculations. It is most sensitive to electron correlation, and thus the computational results in the velocity gauge are most trustworthy.

Inspection of Fig. 1 shows that the photoionization cross sections calculated with three gauges of the electromagnetic operator are quite close near the DPI threshold but gradually diverge with an increase in the photon energy. This result is related to the role which the ground-state correlation plays in two different mechanisms of DPI. The KO mechanism, which is dominant near the threshold, shows little sensitivity to the ground-state correlation. In contrast, the shake-off (SO) mechanism, which takes over near the DPI cross-section maximum, is strongly effected by this type of correlation. As was demonstrated in our earlier work on DPI from the He-like ions [11], it took an extremely accurate and sophisticated 20 term Hylleraas ground-state wave function to reconcile all three gauges of the electromagnetic operator. Unfortunately, such an accurate description is not available for the K-shell electrons in neutral atomic species. On the other hand, our calculations on valence shell DPI from Be and Mg [14] showed that velocity gauge results could be quite reliable even with a medium accuracy MCHF ground state and could match experimental data over a wide range of photon energies [15,16]. Thus, among the three sets of calculations displayed in Fig. 1, we would favor the velocity gauge results.

In Fig. 2 we present the double-to-single photoionization cross-section ratio in Be versus the inverse photon energy. This presentation allows one to see clearly how the double-to-single ratio reaches the asymptotic limit of infinite photon energy. Three panels, from left to right, represent calculations performed with the HF, MCHF, and LeSech ground states. The large photon energy calculations are particularly demanding due to fast oscillations of the continuous state wave functions. In this region, the gauge divergence becomes particularly strong. With the least correlated HF ground state, the length gauge fails completely. The gauge divergence becomes smaller with the more correlated MCHF and LeSech ground states. However, it is still quite noticeable.

The double-to-single photoionization cross-section ratio in the limit of infinite photon energy is calculated using Eq. (4) which relies on the nucleus cusp condition and the value of the ground-state wave function near the origin. As seen
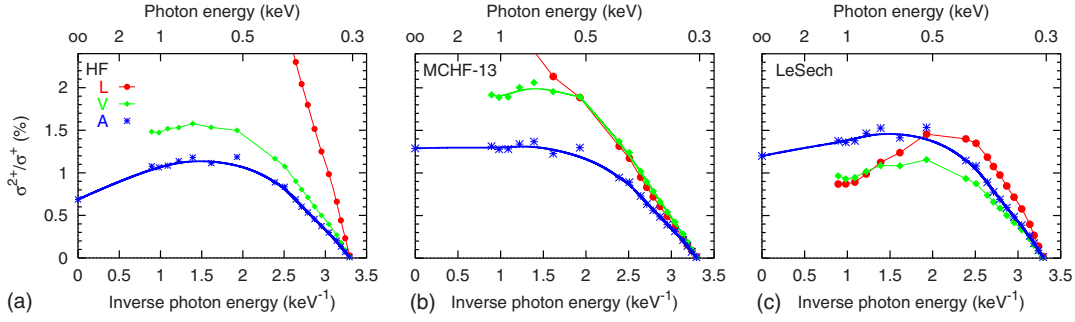
FIG. 2. (Color online) Double-to-single photoionization cross-section ratio in Be versus inverse photon energy calculated with various ground-state wave functions: HF, MCHF, and LeSech (from left to right). The line styles are the same as in Fig. 1.

from Eq. (9), this region of the coordinate space is best accounted for by calculations in the acceleration gauge. That is why we relate the asymptotic ratio to the acceleration gauge calculations at finite photon energies. The blue thick solid line in Fig. 2 represents a polynomial fit bridging the CCC calculation in the acceleration gauge at finite photon energies and the infinite photon energy limit which is reached smoothly.

B. Magnesium

Photoionization cross sections of the K shell of magnesium calculated with a MCHF-11 ground state are presented in Fig. 4. A similar presentation style as in Fig. 1 is used here. Three panels, from left to right, display the single photoionization cross-section $\omega^{7/2}\sigma^{+}$, the double-to-single photoionization cross-section ratio σ^{2+}/σ^{+}, and the DPI cross-section σ^{2+}. The theoretical ratio and the DPI cross section on the central and right panels, respectively, are compared with the experimental data from Hoszowska et al. [8].

The calculations in the three gauges of the electromagnetic operator agree well for the single photoionization cross section. These calculations are consistent with the XCOM data [9]. The calculation with the ATOM program suite [26] is reasonable at the DPI threshold but gradually fails as the photon energy becomes too large. For the DPI cross section, the three gauges of the electromagnetic operator produce quite different results. Based on the arguments presented in Sec. IV A, we trust the velocity gauge results to be most accurate.

Direct comparison with the experiment should be made for the ratio of the double-to-single photoionization cross sections (middle panel of Fig. 3). Our calculation in the velocity gauge agrees reasonably well with the measurement of Hoszowska et al. [8] except for the largest photon energies accessible experimentally. Here, the experimental ratio is noticeably below the theoretical predictions. When the experimental ratio is converted to the DPI cross section by multiplying by the single-ionization cross section [9], disagreement with the theory for larger photon energies looks less dramatic as seen on the right panel of Fig. 3. However, the peak value of the experimental DPI cross section is above the calculation in the velocity gauge.

Hoszowska et al. [8] fitted their data with an empirical KO-SO model and showed that it is the SO mechanism that plays the dominant role at this photon energy range. As the SO process is most sensitive to the ground-state correlation, the disagreement with experiment may be due to an insufficiently accurate ground-state wave function.

In Fig. 4 we present the double-to-single photoionization cross-section ratio in Mg versus the inverse photon energy. As was noted in Sec. IV A, large photon energy calculations display a strong gauge divergence which affects the length gauge in particular. We see the same tendency in the case of Mg. With the least correlated HF ground state, the length gauge fails dramatically. This is cured somewhat with a more correlated MCHF ground state. The gauge divergence at large photon energies is smallest with the LeSech ground state. However, the calculations with this ground state disagree with experiment at moderate photon energies. The ve-
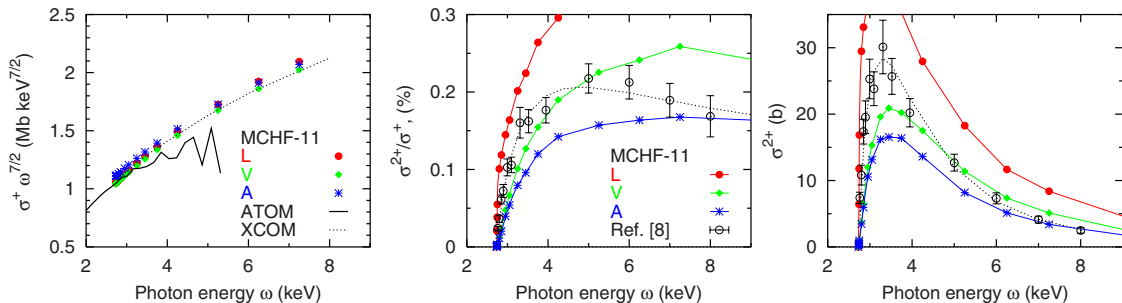

FIG. 3. (Color online) Photoionization cross sections of the K shell of magnesium calculated with the MCHF-11 ground state. Experimental data from [8] are shown with open black circles. The dotted line going through the experimental points is the fit to the data with an empirical KO-SO model. Other line styles are the same as in Fig. 1.
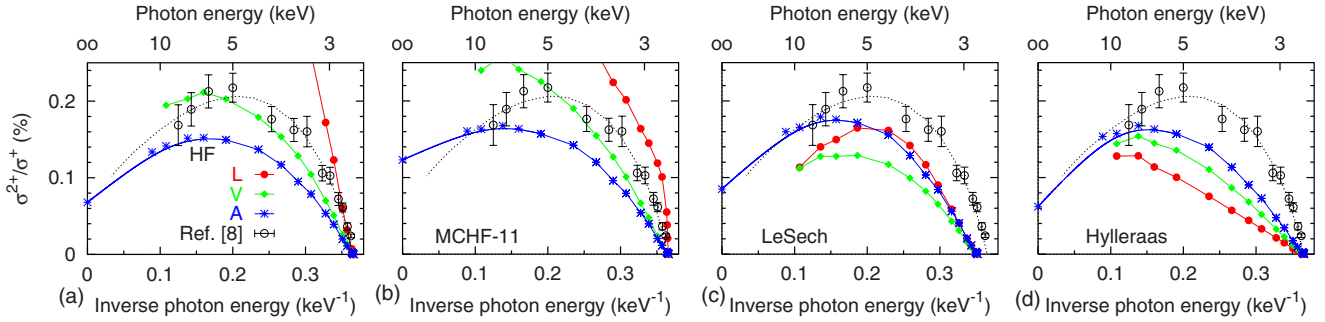
FIG. 4. (Color online) Double-to-single photoionization cross-section ratio in Mg versus inverse photon energy calculated with various ground-state wave functions (from left to right): HF, MCHF, and LeSech of the neutral Mg atom and Hylleraas of the Mg^{10+} ion. The line styles are the same as in Fig. 3.

locity gauge calculation with the HF and MCHF ground states is closest to the experiment.

On the right panel of Fig. 4 we present a hybrid calculation employing a Hylleraas-type ground state of the Mg^{10+} ion [22] and the CCC final state of the neutral Mg atom. This calculation, especially in the acceleration gauge, is fairly similar to an analogous calculation with the LeSech ground state. This is quite understandable since the acceleration gauge enhances the region of the coordinate state close to the nucleus where the electron distribution in the atom and the heliumlike ion is quite similar. Other gauges in the two calculations differ since the two-electron wave functions, both in the initial and final states, are quite different in the two targets away from the nucleus.

C. Calcium

Photoionization cross sections of the K shell of calcium calculated with a MCHF-7 ground state are presented in Fig. 5. A similar presentation style as in Figs. 1 and 3 is used here. Three panels, from left to right, display the single photoionization cross-section $\omega^{7/2}\sigma^+$, the double-to-single photoionization cross-section ratio σ^{2+}/σ^+, and the DPI cross-section σ^{2+}. Single photoionization cross section is consistent with the XCOM data [9]. The theoretical double-to-single ratios on the central panel are compared with the present experimental data and those from Oura *et al.* [3] as well as with the LOPT calculation of Mikhailov *et al.* [7]. The length gauge calculations for the ratio and the DPI cross

section are far off from the other two gauges and have to be scaled down by a factor of 0.3 to fit into the common graph.

Both sets of experimental data are generally consistent within their error bars. Our calculation in the velocity gauge is close to the LOPT calculation of Mikhailov *et al.* [7]. However, the two sets of calculations are markedly below experimental cross-section ratios across the whole range of photon energies. In our valence shell DPI study, we observed that the frozen-core model could fail for Ca because of resonant core excitations. Although we have no direct proof of that, we may speculate that it is the core excitation processes, which are not accounted for in the present frozen-core model that make their contribution to the K-shell DPI process on Ca as well. This could be the reason why theory and experiment disagree so strongly.

In Fig. 6 we present the double-to-single photoionization cross-section ratio in Ca versus the inverse photon energy. As in Fig. 2, three panels, from left to right, represent calculations performed with the HF, MCHF, and LeSech ground states. As in the case of Be and Mg, the double-to-single ratio displays a strong gauge divergence at large photon energies when calculated with the HF and MCHF ground states. The length gauge is particularly divergent and has to be scaled down by a factor of 0.3 with both ground states. A more correlated MCHF ground state seems to cure somewhat this divergence at very large photon energies but the need for rescaling remains. The LeSech ground state does not suffer that much from the gauge divergence. The MCHF calculation in the velocity gauge and the LeS calculation in the
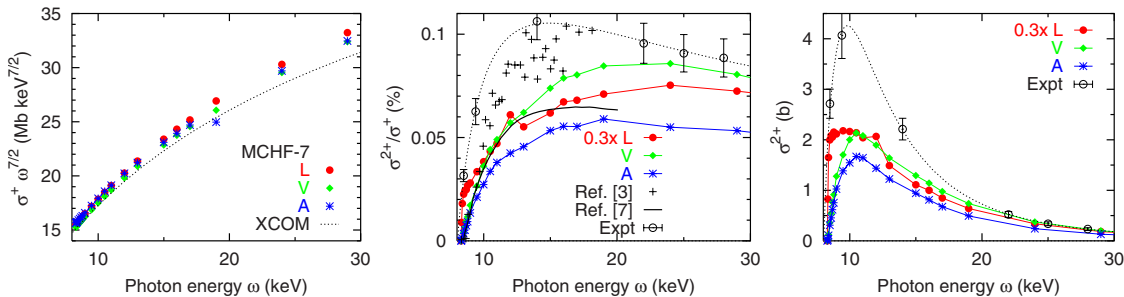

FIG. 5. (Color online) Photoionization cross sections of the K shell of calcium calculated with the MCHF-7 ground state. Experimental data from [3] are shown on the middle panel with crosses. The black solid line represents the LOPT calculation of Mikhailov *et al.* [7]. Present experimental data are shown with open circles. The dotted line is the fit to the data with an empirical SO-KO model. Other line styles are the same as in Fig. 1.
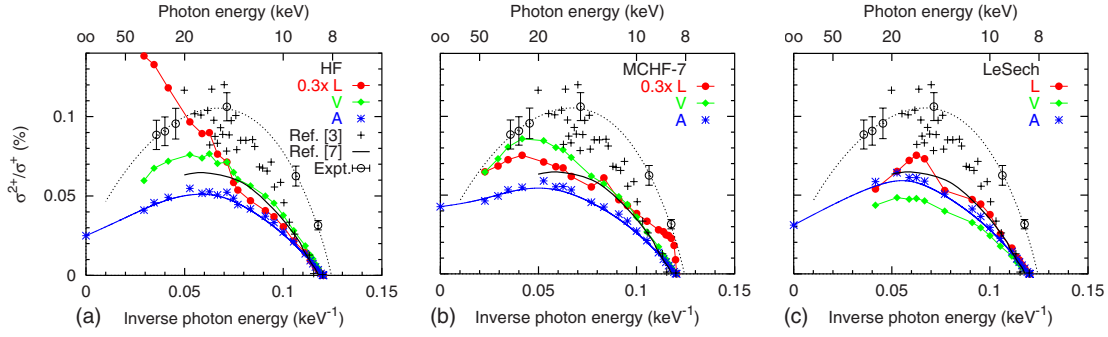
FIG. 6. (Color online) Double-to-single photoionization cross-section ratio in Ca versus inverse photon energy calculated with various ground-state wave functions: HF, MCHF, and LeSech (from left to right). The line styles are the same as in Figs. 2 and 4.

acceleration gauge are consistent with the LOPT calculation of Mikhailov *et al.* [7] but our ratios are well below the experimental values.

D. Scaling laws

It was established by Kornberg and Miraglia [10] that the DPI cross section in the helium isoelectronic sequence of ions follows a universal scaling law when plotted in the reduced coordinates $\sigma^{2+} Z^4$ vs $\Delta E/Z^2$. Hoszowska *et al.* [8] extended this law to the K-shell DPI of neutral Mg, Al, and Si atoms by introducing effective charges Z^*. These charges were obtained from the energy of the K shell of a singly-charged ion fitted with a hydrogenic formula $\epsilon_{1s}^+(\mathrm{Ry})=Z^{*2}$. For the He isoelectronic sequence of ions, $Z^*=Z$. In Table I we present the energies ϵ_{1s}^+ (labeled as second ionization potential) and corresponding effective charges Z^* derived from MCHF calculations on the corresponding singly-charged ion with a K hole.

In Fig. 7 we use the effective charges Z^* from Table I to test the DPI cross sections of Be, Mg, and Ca, calculated with HF, MCHF, and LeSech ground states, against the scaling law $\sigma^{2+} Z^{*4}$ vs $\Delta E/Z^{*2}$, where the excess energy $\Delta E=\omega-IP^{2+}$ is calculated using the DPI thresholds from Table I.

We see from Fig. 7 that the proposed scaling law does indeed hold across the studied sequence of the alkaline-earth metal atoms. The most accurate scaling is exhibited by the velocity gauge calculation with the least correlated HF

ground states. A more correlated MCHF ground state produces good scaling at large excess energies but the DPI of all three atoms diverges near the threshold. The theoretical DPI of magnesium tends to follow closer to the experimental data of Hoszowska *et al.* [8]. The velocity gauge DPI results with the LeSech ground state are far too low for all three atoms. So we choose to scale the acceleration gauge results. The quality of such a scaling is somewhat in between of that with the HF and MCHF ground states.

Because of the screening of the nucleus from the K shell by the rest of atomic electrons, the effective charge Z^* is smaller than the bare nucleus charge Z. However, even with this effect taken into account, the scaling of the neutral atoms is quite different from that of the corresponding members of the helium isoelectronic sequence of ions. Hoszowska *et al.* [8] suggested that the scaled DPI of the neutral atoms can be reconciled with the family of the He-like ions by reducing slightly the power of the effective charge from 4 to 3.68. This is clearly seen in Fig. 8 where we compare the experimental data for the K shell of the neutral Mg [8] and Ca atoms with the theoretical cross sections of the heliumlike ions Be^{2+}, Mg^{10+}, Al^{11+}, and Si^{12+}. Because of the very large photon energies, we could not run a CCC calculation on the Ca^{18+} ion. Nevertheless, all the studied members of the helium isoelectronic sequence of ions fit very well to the same curve. When the effective charge power is properly adjusted, the K-shell family of the neutral atoms does indeed approach this curve quite closely.
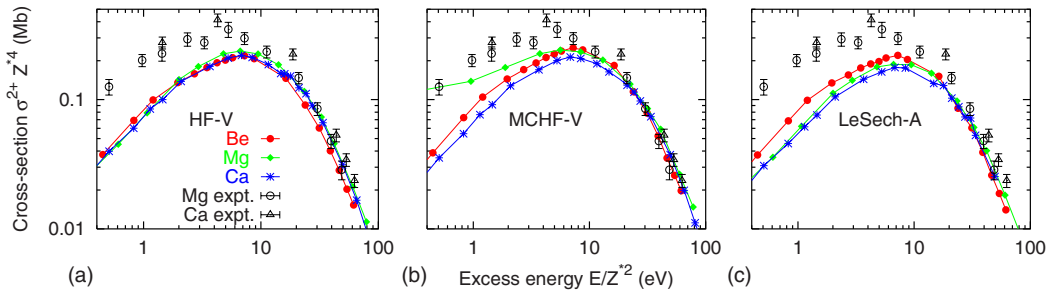

FIG. 7. (Color online) Scaled double photoionization cross-section $\sigma^{2+} Z^{*4}$ of the K shells of Be (red circles), Mg (green diamonds), and Ca (blue asterisks) plotted versus the excess energy $\Delta E/Z^{*4}$ above the respective DPI threshold. The three panels (from left to right) display calculations with the HF, MCHF (in the velocity gauge), and the LeSech ground states in the acceleration gauge. The experimental data for Mg from Hoszowska *et al.* [8] (open circles) and present experimental data for Ca (open triangles) are plotted with error bars.
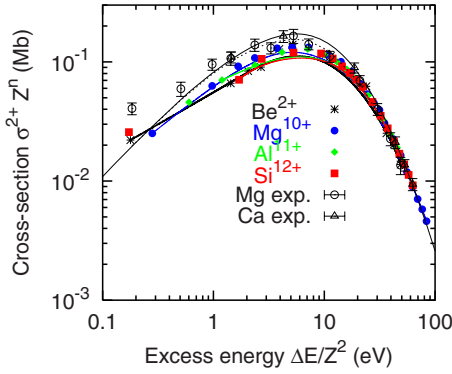
FIG. 8. (Color online) Scaled double photoionization cross-section $\sigma^{2+} Z^4$ of the K shell of heliumlike ions Be^{2+} (black asterisks), Mg^{10+} (blue filled circles), Al^{11+} (green diamonds), and Si^{12+} (red squares) are plotted versus the excess energy $\Delta E/Z^4$. The solid lines are drawn to guide the eyes. The experimental data for Mg from Hoszowska *et al.* [8] (open circles) and present experimental data for Ca (open triangles) in the $\sigma^{2+} Z^{*3.68}$ vs $\Delta E/Z^{*2}$ coordinates are plotted with error bars. The dotted and solid lines joining the experimental points for Mg and Ca, respectively, are the SO-KO fit to the data.

V. CONCLUSION

In the present paper, we studied the K-shell double photoionization of light alkaline-earth metal atoms: Be, Mg, and Ca. The theoretical single and double photoionization cross sections were obtained using the convergent close-coupling method and employing different ground-state wave functions of various degrees of correlation. The single photoionization cross sections were tested against the reference data from the XCOM database [9] which served as a useful check of accuracy of calculations which were performed in three gauges of the electromagnetic operator: length, velocity, and acceleration. Away from threshold, the DPI cross sections for all the studied atoms suffered from gauge divergence, especially strong in the length gauge. Nevertheless, the combination of

the velocity gauge with the HF and MCHF ground states, and the acceleration gauge with LeSech ground state, produced sensible results for the double-to-single photoionization cross-section ratio and the DIP cross section. Some advantage of the velocity gauge can be attributed to a well-balanced contribution of various regions of the coordinate space into the calculations of radial integrals. The LeSech ground state, by design, was specially optimized to reproduce best the electron distribution in the innermost K shell and ignored completely the outer core and valence electrons. Thus, it was found to be most suitable for the acceleration gauge calculations which spanned this region of the coordinate space most accurately.

The universal scaling law was tested in the reduced coordinates $\sigma^{2+} Z^{*4}$ vs $\Delta E/Z^{*2}$, where the effective charges were deduced from the second ionization potential of the corresponding K shell. The scaling law was upheld, with various degrees of accuracy, depending on the description of the atomic ground state. Further, the K-shell DPI scaling curve for neutral atomic species was compared with analogous scaling of the He-like ions. Both families of targets could be placed on a universal scaling curve if the neutrals were scaled as $\sigma^{2+} Z^{*3.68}$ as suggested by Hoszowska *et al.* [8].

The present work attempts a systematic study of the K-shell DPI using an *ab initio* nonperturbative method. It shows significant difficulties of such a calculation which is particularly demanding to the accuracy of the ground state. Thus far, none of the available ground-state wave functions satisfied the strict gauge convergence test. Nevertheless, the authors are hopeful that the present report will stimulate further efforts approaching the problem from both experimental and theoretical sides.

[1] J. S. Briggs and V. Schmidt, J. Phys. B **33**, R1 (2000).

[2] L. Avaldi and A. Huetz, J. Phys. B **38**, S861 (2005).

[3] M. Oura *et al.*, J. Phys. B **35**, 3847 (2002).

[4] S. Huotari, K. Hämäläinen, R. Diamant, R. Sharon, C. C. Kao, and M. Deutsch, Phys. Rev. Lett. **101**, 043001 (2008).

[5] E. P. Kanter, I. Ahmad, R. W. Dunford, D. S. Gemmell, B. Krassig, S. H. Southworth, and L. Young, Phys. Rev. A **73**, 022708 (2006).

[6] S. H. Southworth, E. P. Kanter, B. Krässig, L. Young, G. B. Armen, J. C. Levin, D. L. Ederer, and M. H. Chen, Phys. Rev. A **67**, 062712 (2003).

[7] A. I. Mikhailov, I. A. Mikhailov, A. N. Moskalev, A. V. Nefiodov, G. Plunien, and G. Soff, Phys. Rev. A **69**, 032703 (2004).

[8] J. Hoszowska *et al.*, Phys. Rev. Lett. **102**, 073006 (2009).

[9] M. Berger, J. Hubbell, S. Seltzer, J. Chang, J. Coursey, R. Sukumar, and D. Zucker, *XCOM: Photon Cross Sections Database*, 1st ed. (National Institute of Standards and Technology, Gaithersburg, MD, 2005).

[10] M. A. Kornberg and J. E. Miraglia, Phys. Rev. A **48**, 3714 (1993).

[11] A. S. Kheifets and I. Bray, Phys. Rev. A **58**, 4501 (1998).

[12] T. Schneider and J.-M. Rost, Phys. Rev. A **67**, 062704 (2003).

[13] R. C. Forrey, H. R. Sadeghpour, J. D. Baker, J. D. Morgan, and A. Dalgarno, Phys. Rev. A **51**, 2112 (1995).

[14] A. S. Kheifets and I. Bray, Phys. Rev. A **75**, 042703 (2007).

[15] R. Wehlitz, D. Lukic, and J. B. Bluett, Phys. Rev. A **71**, 012707 (2005).

[16] R. Wehlitz, P. N. Juranić, and D. V. Lukić, Phys. Rev. A **78**, 033428 (2008).

[17] A. S. Kheifets and I. Bray, Phys. Rev. A **57**, 2590 (1998).

[18] K. G. Dyall, I. P. Grant, C. T. Johnson, F. P. Parpia, and E. P. Plummer, Comput. Phys. Commun. **55**, 425 (1989).

[19] D. M. Mitnik and J. E. Miraglia, J. Phys. B **38**, 3325 (2005).

[20] M. Becher, B. Joulakian, C. Le Sech, and M. Chrysos, Phys. Rev. A **77**, 052710 (2008).

[21] A. Dalgarno and A. L. Stewart, Proc. Phys. Soc. London **76**, 49 (1960).

[22] J. F. Hart and G. Herzberg, Phys. Rev. **106**, 79 (1957).

[23] I. Bray, Phys. Rev. A **49**, 1066 (1994).

[24] M. Y. Amusia, *Atomic Photoeffect* (Plenum, New York, 1990).

[25] J. Hoszowska, J. C. Dousse, J. Kern, and C. Rheme, Nucl. Instrum. Methods Phys. Res. A **376**, 129 (1996).

[26] M. I. Amusia and L. V. Chernysheva, *Computation of Atomic Processes: A Handbook for the ATOM Programs* (Institute of Physics, Bristol, UK, 1997).